Twin-Twisted van der Waals Crystal for Entangled Photon Source

Chaojie Ma,[1,2,*] Mingkang Zhang,[1,*] Lu He,[3,*] Yijun Wang,[1] Xuping Shi,[1] Chang Liu,[4] Youbao Ni,[5] Haixin Wu,[5] Yun-Kun Wu,[6,7] Xifeng Ren,[6,7] Zhipei Sun,[8] Ling-Jun Kong,[3,†] Xiangdong Zhang,[3,‡] Hao Hong,[1,9,§] and Kaihui Liu[1,4,10,∥]

[1]*State Key Lab for Mesoscopic Physics and Frontiers Science Center for Nano-optoelectronics, School of Physics, Peking University, Beijing, China*
[2]*Beijing National Laboratory for Condensed Matter Physics, Institute of Physics, Chinese Academy of Sciences, Beijing, China*
[3]*Key Laboratory of advanced optoelectronic quantum architecture and measurements of Ministry of Education, Beijing Key Laboratory of Nanophotonics and Ultrafine Optoelectronic Systems, School of Physics, Beijing Institute of Technology, Beijing, China*
[4]*International Centre for Quantum Materials, Collaborative Innovation Centre of Quantum Matter, Peking University, Beijing, China*
[5]*Anhui Institute of Optics and Fine Mechanics, Hefei Institutes of Physical Science, Chinese Academy of Sciences, Hefei, China*
[6]*Laboratory of Quantum Information, University of Science and Technology of China, Hefei, China*
[7]*Hefei National Laboratory, University of Science and Technology of China, Hefei, China*
[8]*QTF Centre of Excellence, Department of Electronics and Nanoengineering, Aalto University, Espoo, Finland*
[9]*Beijing Key Laboratory of Advanced Micro- and Nanoscale Light Source Materials and Devices, Peking University, Beijing, China*
[10]*Interdisciplinary Institute of Light-Element Quantum Materials and Research Centre for Light-Element Advanced Materials, Peking University, Beijing, China*

(Received 2 December 2025; revised 20 April 2026; accepted 22 July 2026; published 20 August 2026)

Bright entangled photon sources with on-demand quantum state control are essential for advancing quantum science and technologies. However, simultaneously achieving high brightness and state tunability remains challenging, as this necessitates a dual-phase control mechanism that facilitates both longitudinal phase matching and transverse polarization modulation. Here, we report a twin-twisted two-dimensional (2D) van der Waals (vdW) crystal architecture that enables spontaneous parametric down-conversion (SPDC) with both high generation efficiency and continuously tunable quantum states. The designed crystal comprises two sections of twisted 2D GaSe vdW flakes with opposite chiral handedness, in which interflake twist angle induces phase matching in SPDC, and intersection twisting provides an additional degree of freedom on tunability. We demonstrate that the twin-twisted GaSe crystals achieve a record-high photon-pair generation rate exceeding 13 200 Hz and a Bell state fidelity above 99% within 2D material family, and enable unprecedented tunability of quantum states from the maximally polarization entangled states to the fully separable states. This study opens a practical avenue toward twist-engineered quantum states, and paves the way for developing compact quantum photonic systems with tailored properties.

DOI: 10.1103/wp59-zvvb

Spontaneous parametric down-conversion (SPDC) in noncentrosymmetric crystals, in which the second-order nonlinear susceptibility $\chi^{(2)}$ is nonzero, has long served as the cornerstone for generating entangled photon pairs since the late 20th century [1,2]. Over the past few decades, SPDC sources have evolved with the characteristics of ultrahigh brightness, high-dimensional and multiphoton entanglement, leading to key advances in quantum mechanics and emerging quantum technologies [3–11]. However, realizing SPDC sources that offer both high generation efficiency and versatile quantum state control—essential for quantum communication, computing, and imaging—remains a fundamental challenge. Typically, efficient SPDC relies on birefringent- or quasi-phase-matching schemes to ensure momentum conservation among the interacting waves. However, conventional birefringent and polar materials, such as bulk beta barium borate (BBO) and lithium niobate ($LiNbO_3$), generally support only one dominant $\chi^{(2)}$ tensor component, thus inherently constraining the versatility and tunability of the generated quantum states. Recently, great success has been achieved

[*]These authors contributed equally to this work.
[†]Contact author: konglj@bit.edu.cn
[‡]Contact author: zhangxd@bit.edu.cn
[§]Contact author: haohong@pku.edu.cn
[∥]Contact author: khliu@pku.edu.cn

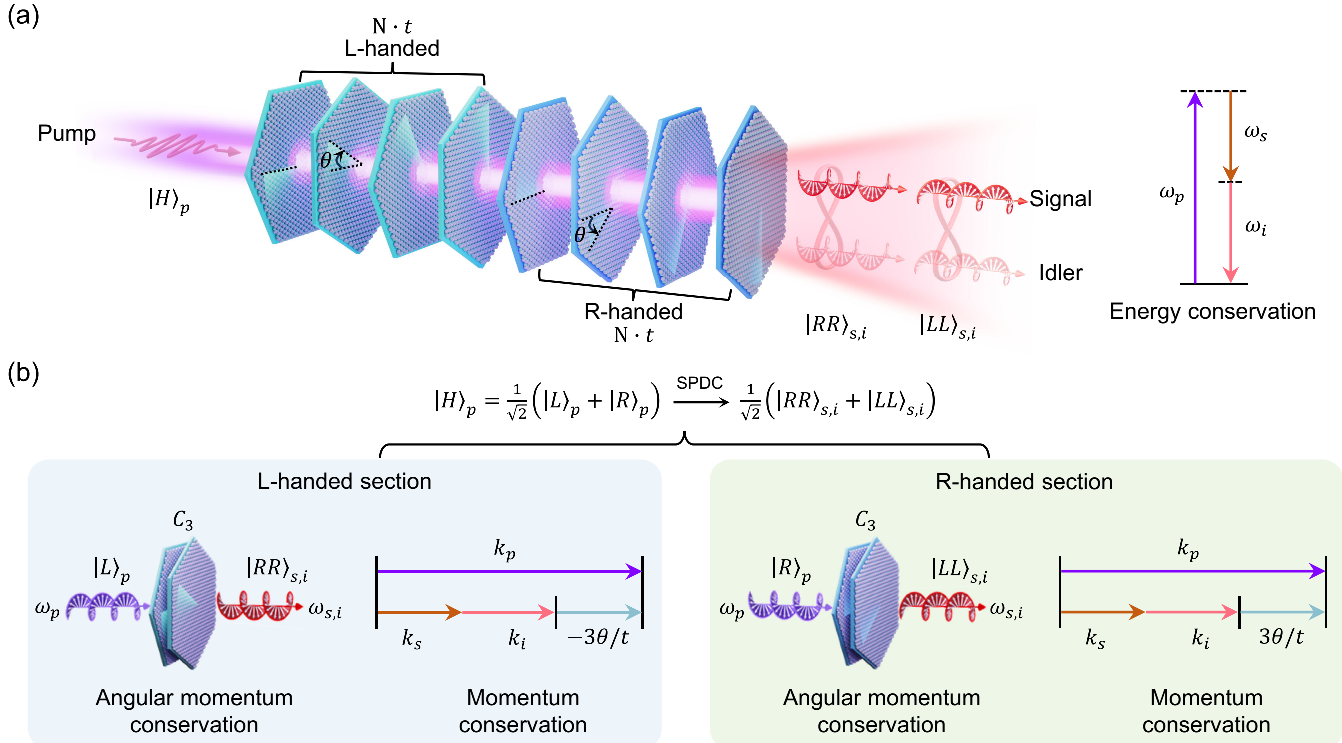

FIG. 1. Principle of entangled state generation in designed twin-twisted vdW crystal. (a) Illustration of SPDC for the polarization-entangled state generation in a twin-twisted crystal assembled from LH and RH sections. Each section is constructed from N pieces of C_3 symmetric flakes with identical thicknesses t and interflake twist angles θ for phase-matching. In the SPDC process, one pump photon with a frequency of ω_p is split into signal and idler photons with frequency of ω_s and ω_i, following energy conservation. (b) Schematic of the SPDC process in LH and RH sections. Here, the LH (RH) section can respond only to left (right) circular polarization $|L\rangle_p$ ($|R\rangle_p$) pump to emit photon pairs in the state $|RR\rangle_{s,i}$ ($|LL\rangle_{s,i}$). Thus, under a pump of $|H\rangle_p$, the twin-twisted crystal enables the generation of the maximally polarization-entangled state $|\psi\rangle = \frac{1}{\sqrt{2}}(|RR\rangle_{s,i} + |LL\rangle_{s,i})$.

in metasurfaces and liquid crystals [12,13], which offer multiple tensor components that enable the generation and engineering of diverse quantum states under a relaxed phase-matching condition. Nevertheless, such relaxation comes at the cost of reduced generation efficiency.

Two-dimensional (2D) van der Waals (vdW) materials with unique out-of-plane vdW coupling and pronounced in-plane $\chi^{(2)}$ are emerging as promising platforms for compact, integrated photonic devices operating across classical and quantum regimes [14–18]. Recent studies have revealed that the grown 2D layers can be vertically stacked with aligned crystallographic orientations, thereby preserving broken inversion symmetry in vdW crystals [19–26]. This unique structure enables the scaling of second-order nonlinear optical responses with the number of layers and thereby facilitates the realization of SPDC in thin 2D vdW crystals [27–35]. Notably, 2D crystals such as rhombohedral-phase (3R) MoS_2 and BN, which exhibit threefold rotational (C_3) symmetry, possess four in-plane identical nonzero $\chi^{(2)}$ tensor components, thus inherently supporting the generation of polarization-entangled Bell states [28,33]. The photon-pair generation efficiency can be substantially enhanced through 180° inversion-twist stacking of adjacent flakes to achieve quasi-phase-matching [30,35]. Nonetheless, the influence of the twist angle—a central degree of freedom in 2D vdW systems—on the resulting entangled quantum states remains merely investigated.

Twist engineering in 2D vdW crystals has recently been demonstrated to induce nonlinear geometric phases and to enable phase matching in second harmonic generation (SHG) [36]. Here, we demonstrate that the twist angle can strikingly serve as a dual control knob for phase matching and polarization-entangled state modulation in SPDC. This control is enabled by our engineered twin-twisted crystal architecture, composed of two chiral sections formed by left-handed (LH) and right-handed (RH) vdW flakes. We experimentally fabricate the twin-twisted GaSe crystal, which generates high-brightness entangled photon pairs at a rate exceeding 13 200 Hz, achieves a Bell state fidelity of up to 99%, and allows for the continuous tuning of both the amplitude and phase of the quantum states.

We begin by introducing the design principle of the efficient polarization entanglement photon source based on SPDC in a twin-twisted 2D vdW crystal with C_3 symmetry. The crystal comprises two chiral sections, namely,

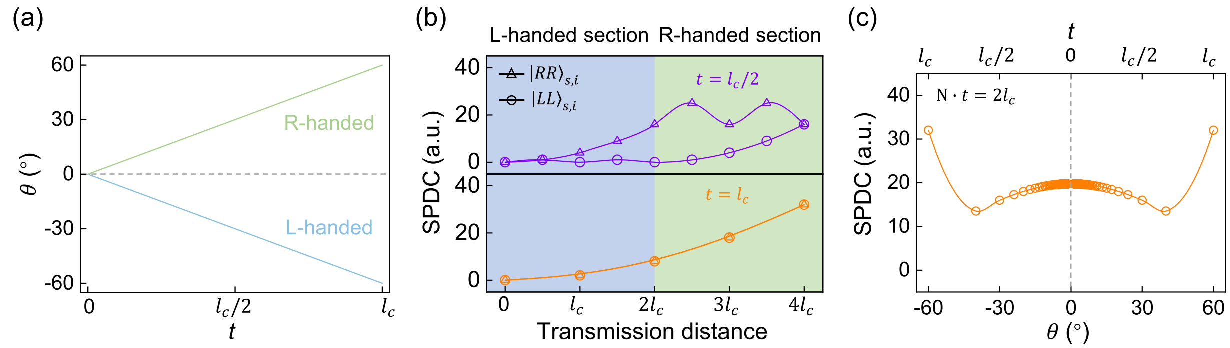

FIG. 2. Flake thickness and twist angle dependence of SPDC response in twin-twisted vdW crystal. (a) Twist-phase-matching conditions of the flake thicknesses t and twist angles θ in the SPDC process. (b) Calculated SPDC efficiency in twin-twisted crystal under two different phase-matching conditions. For $t = l_c/2$, LH (RH) section responds exclusively to $|L\rangle_p$ ($|R\rangle_p$) pump to emit $|RR\rangle_{s,i}$ ($|LL\rangle_{s,i}$) photons and exhibits the same efficiency through the twin-twisted crystal with a thickness of $4l_c$. For $t = l_c$, SPDC occurs in both sections with the same probability and the efficiency increases quadratically with flake number. (c) Flake thickness and twist angle dependence of SPDC efficiency for twin-twisted crystals with a total thickness of $4l_c$.

LH and RH sections, each constructed from N pieces of flakes with identical thicknesses t and interflake twist angles θ [Fig. 1(a)]. The LH section features an anticlockwise rotation of the stacking flakes along the direction of the pump light (where θ is defined as negative), whereas the RH section features a clockwise rotation (where θ is defined as positive).

In this design, three selection laws govern the SPDC process, i.e., energy conservation, angular momentum conservation, and momentum conservation [Figs. 1(a) and 1(b)]. With respect to energy conservation, a pump photon with frequency ω_p undergoes the SPDC process, resulting in the generation of signal and idler photons with frequency of ω_s and ω_i, with $\omega_p = \omega_s + \omega_i$. For angular momentum conservation, the SPDC governed by the C_3 symmetric crystal can be expressed as $\sigma_p\hbar - \sigma_s\hbar - \sigma_i\hbar = 3\mathrm{M}\hbar$, where $\sigma_p\hbar$, $\sigma_s\hbar$, and $\sigma_i\hbar$ separately denote the spin angular momenta (here $\sigma = \pm 1$, corresponding to the left and right circular polarization) of pump, signal and idler photons, M denotes an integer, and $3\mathrm{M}\hbar$ denotes the angular momentum imparted by the crystal. Therefore, the C_3 symmetric crystal enables down-converted photons with the opposite circular polarization states as that of the pump photon [37,38]. Momentum conservation is achieved through interflake rotations at a specific twist angle for phase matching. An interflake twist can induce a geometric phase under a left or right circular polarization pump ($|L\rangle_p/|R\rangle_p$) in classical second-order nonlinear processes [36,39]. The geometric phase can also be applied to compensate for the phase mismatch in SPDC process (Supplemental Material [40]), as follows:

$$k_s + k_i + 3|\theta|/t = k_p, \tag{1}$$

where k_p, k_s, and k_i separately denote the wave vectors of pump, signal, and idler photons.

In our designed twin-twisted crystal, the LH (RH) section responds to the $|L\rangle_p$ ($|R\rangle_p$) to emit the down-converted photon pairs $|RR\rangle_{s,i}$ ($|LL\rangle_{s,i}$). Thus, under horizontal polarization excitation of $|H\rangle_p = \frac{1}{\sqrt{2}}(|L\rangle_p + |R\rangle_p)$, the pump photons can undergo down-conversion in either section with the same probability. Since the spatial modes of the emitted photons remain indistinguishable across sections, these SPDC processes are coherently superposed, forming a maximally polarization-entangled state, which can be expressed as

$$|\psi\rangle = \frac{1}{\sqrt{2}}(|RR\rangle_{s,i} + |LL\rangle_{s,i}). \tag{2}$$

The generation efficiency of SPDC depends on the flake thickness t and interflake twist angle θ of the designed twin-twisted crystal. The twist-phase-matching conditions described in Eq. (1) establish the following relationship between θ and t [Fig. 2(a); Supplemental Material [40]]:

$$\theta = \mp 60^\circ \cdot \frac{t}{l_c}, \tag{3}$$

where l_c ($l_c = \pi/\Delta k$, $\Delta k = k_p - k_s - k_i$) denotes the coherence length for the SPDC process, and the $-$ and $+$ signs correspond to the defined LH and RH sections, respectively. The generation efficiency of the SPDC process can be calculated as follows (Supplemental Material [40]):

$$\eta_{\mathrm{SPDC}} \propto \begin{cases} \left[T\mathrm{sinc}\left(\frac{\Delta k t}{2}\right)\right]^2, t < l_c \\ \left[2T\mathrm{sinc}\left(\frac{\Delta k t}{2}\right)\right]^2, t = l_c \end{cases}, \tag{4}$$

where $T = 2\mathrm{N}\cdot t$ denotes the total thickness of the twin-twisted crystal. For $t < l_c$, SPDC occurs exclusively in one chiral section, yielding either $|RR\rangle_{s,i}$ or $|LL\rangle_{s,i}$ [Fig. 2(b)]. At a fixed total thickness of T, the efficiency increases

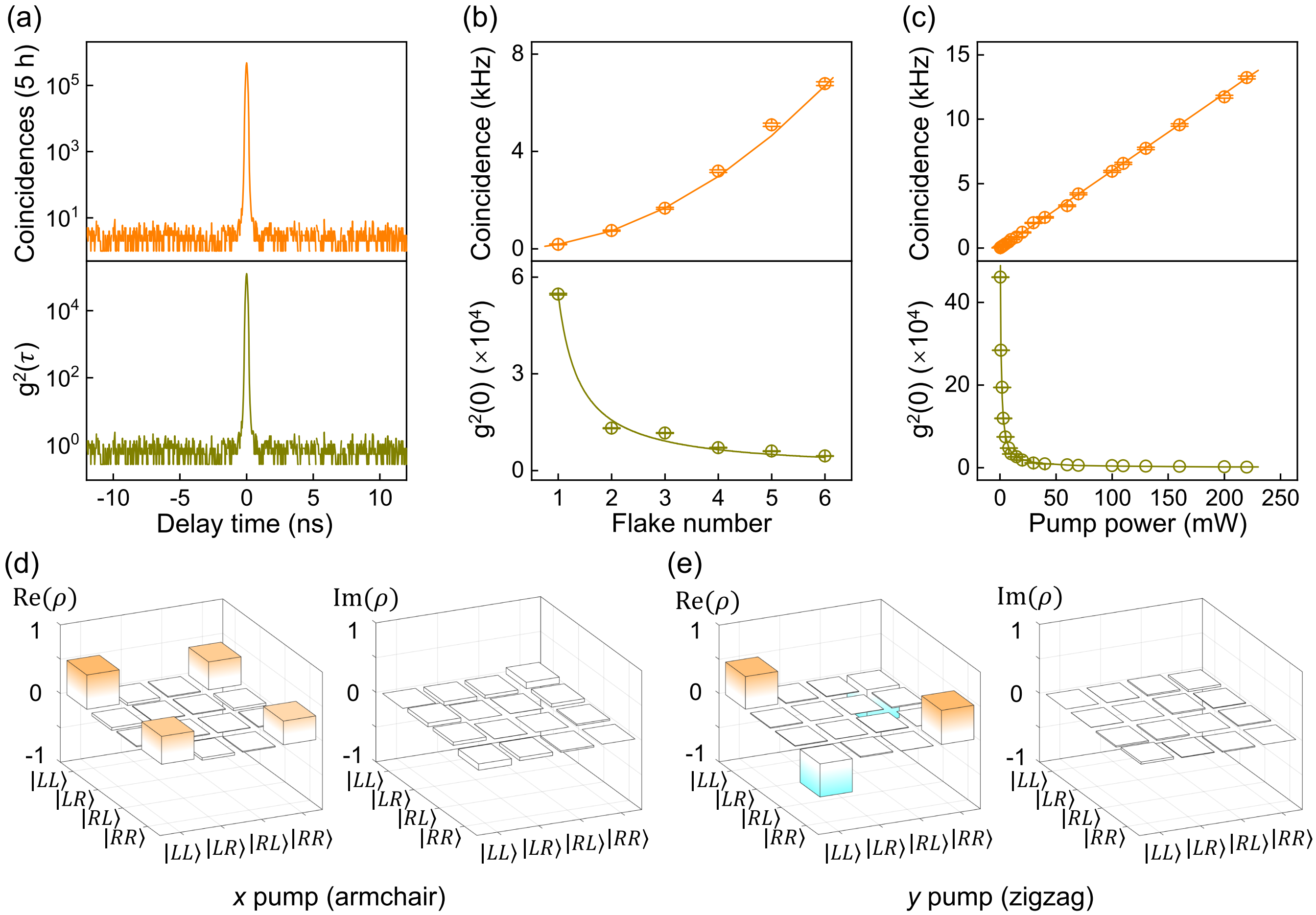

FIG. 3. Efficient generation of polarization-entangled Bell states in twin-twisted GaSe crystals. (a) Measured coincidences (top panel) and second-order correlation function $g^{(2)}(\tau)$ (bottom panel) for twin-twisted sample with an integration time of 5 h. (b) Flake number dependence of the coincidence rate (top panel) and second-order correlation function $g^{(2)}(0)$ (bottom panel). The coincidence rate scales quadratically with the number of flakes, consistent with the phase-matching theory. Notably, $g^{(2)}(0)$ decreases with increasing flake number, due to the increase in accidental counts. (c) Power dependence of the coincidence rate (top panel) and $g^{(2)}(0)$ (bottom panel). The coincidence rate and $g^{(2)}(0)$ exhibit linear and reversal relationships with power, respectively. The error bars indicate the standard deviations calculated from the Poissonian statistic. (d),(e) Measured density matrices ρ for the linear polarization pump along the x (armchair) direction (d) and y (zigzag) direction (e). The reconstructed density matrices in (d) and (e) are highly consistent with the expected Bell states $1/\sqrt{2}(|RR\rangle_{s,i} + |LL\rangle_{s,i})$ and $1/\sqrt{2}(|RR\rangle_{s,i} - |LL\rangle_{s,i})$, respectively. Both the real and imaginary parts [Re(ρ) and Im(ρ)] are given.

correspondingly with decreasing t [Fig. 2(c)]. For $t = l_c$, the configuration is a singularity, in which the LH and RH sections evolve into an achiral configuration. In this scenario, SPDC for $|RR\rangle_{s,i}$ and $|LL\rangle_{s,i}$ occurs in both sections with the same probability, and the efficiency increases quadratically with the flake number [Fig. 2(b)]. Thus, a characteristic "W"-shaped dependence of the SPDC efficiency on t can be observed from our simulations, with the maximum efficiency occurring at $t = l_c$ [Fig. 2(c)].

Experimentally, the ε-GaSe crystal with C_3 symmetry is selectively adopted (Supplemental Material [40] Fig. S1), leveraging its high in-plane $\chi^{(2)}$ value [46]. The twin-twisted GaSe crystals are fabricated onto the fused silica substrate, and a 780-nm continuous-wave laser is used as a pump source to generate entangled photon pairs around 1560 nm (Supplemental Material [40]). The typical coincidences and the second-order correlation function $g^{(2)}(\tau)$ for a six-flake twisted GaSe crystal, with each flake thickness of $t = l_c = 3.55$ μm and interflake twist angle of $\theta = 60°$, are given in Fig. 3(a). An extremely high two-photon correlation peak $g^{(2)}(0)$ can be observed at a pump power of ∼2 mW, with a coincidence-to-accidental ratio (CAR) [defined as $g^{(2)}(0) - 1$] exceeding 10^5, revealing nearly ideal photon-pair generation with negligible background noise.

Twist-phase-matching design is robust against angular misalignments and allows a coherent enhancement in the generation rate with increasing number of flakes (Supplemental Material [40] Figs. S2 and S3). The photon-pair coincidence rate exhibits a quadratic dependence

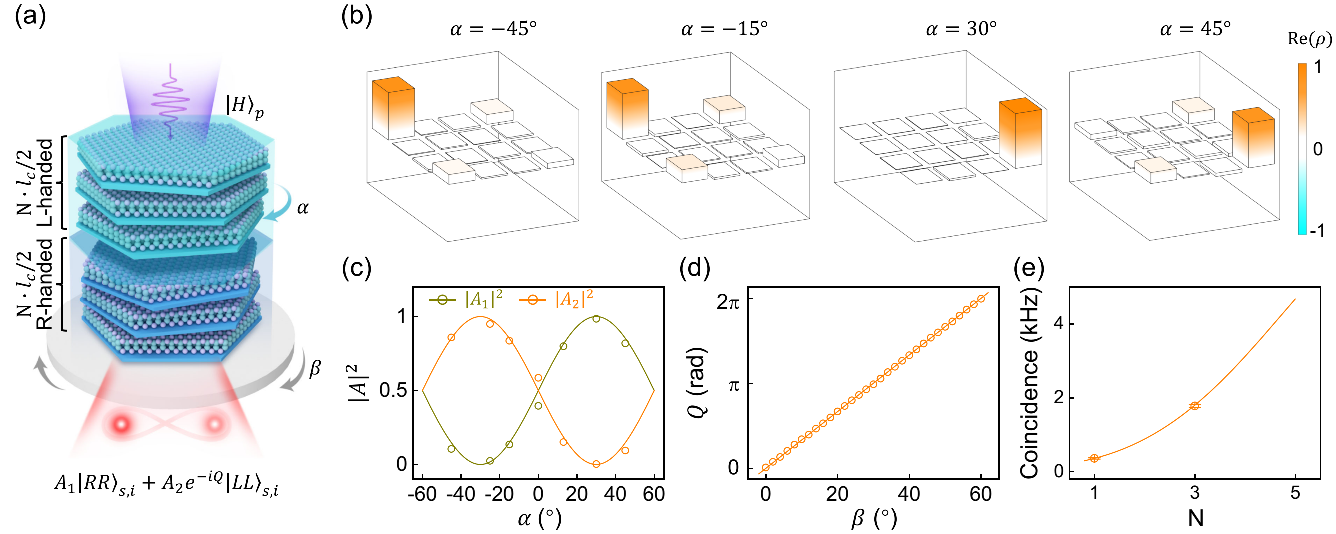

FIG. 4. Twist-engineered polarization entanglement states in twin-twisted GaSe crystal. (a) Schematic of the tuning of two-photon quantum states with α and β of the twin-twisted crystal. (b) Real parts of the measured density matrices ρ under different α. With $\beta = 0°$, the reconstructed density matrices evolve correspondingly with $\alpha = -45°, -15°, 30°, 45°$. (c) Theoretical (solid lines) and experimental (dots) results for the amplitudes of quantum states as functions of α. $|A_1|^2$ and $|A_2|^2$ follow a sinusoidal relationship with α, but with a constant summation. (d) Theoretical (solid lines) and experimental (dots) results for the quantum state phase tuning as a function of β. The phase Q follows a linear relationship with β. (e) Flake number N in (a) dependence of the coincidence rate as $t = l_c/2$. The error bars indicate the standard deviations calculated from the Poissonian statistic.

on the flake number, as expected [Fig. 3(b), top panel]. With increasing pump power, a generation rate of over 13 200 Hz is achieved for the six-flake stacked GaSe crystal [Fig. 3(c), top panel]. Moreover, $g^{(2)}(0)$ is inversely related to the number of flakes [Fig. 3(b), bottom panel] and pump power [Fig. 3(c), bottom panel], reflecting the trade-off between the generation rate and noise level.

Quantum state tomography measurements are performed to reconstruct the density matrices of the entangled states generated from the six-flake stacked GaSe crystal (Supplemental Material [40] Figs. S4 and S5). When the pump polarization is oriented along the x (armchair) or y (zigzag) direction, the reconstructed density matrix ρ is highly consistent with the expected Bell state $1/\sqrt{2}(|RR\rangle_{s,i} + |LL\rangle_{s,i})$ or $1/\sqrt{2}(|RR\rangle_{s,i} - |LL\rangle_{s,i})$ [Figs. 3(d) and 3(e)]. Here, the fidelities of the generated quantum states are $97.5 \pm 0.1\%$ and $99.4 \pm 0.1\%$, respectively. To our knowledge, the performance of our compact entangled photon-pair source in terms of the generation rate, CAR, and fidelity is record-high among 2D vdW materials (Supplemental Material [40] Table S1).

The quantum states can be controlled via the twin-twisted design by tuning the relative rotation angle α (the angle between the LH and RH sections) and the relative azimuth angle β (the angle between the $|H\rangle_p$ and the armchair direction of the bottom flake), as shown in Fig. 4(a). The unnormalized quantum state $|\psi\rangle$ of photon pairs can be expressed as (Supplemental Material [40]):

$$|\psi\rangle = \left[\mathrm{N} + \frac{1 - e^{i2\mathrm{N}\Delta kt}}{1 - e^{i2\Delta kt}} e^{i(-3\alpha + \Delta kt)}\right] |RR\rangle_{s,i} + \left[\frac{1 - e^{i2\mathrm{N}\Delta kt}}{1 - e^{i2\Delta kt}} + \mathrm{N}e^{i(3\alpha + 2\mathrm{N}\Delta kt - \Delta kt)}\right] e^{-i6(\alpha+\beta)} |LL\rangle_{s,i}. \tag{5}$$

Thus, both the amplitude and phase of the quantum states can be engineered by α and β.

For simplification, we demonstrate a situation where each section comprises an odd number of stacking flakes with a specific thickness of $t = l_c/2$. The quantum state $|\psi\rangle$ can be simplified as

$$|\psi\rangle = A_1|RR\rangle_{s,i} + A_2e^{-iQ}|LL\rangle_{s,i}, \tag{6}$$

where $A_1 = \sqrt{\mathrm{N}^2 + 2\mathrm{N}\sin 3\alpha + 1}$, $A_2 = \sqrt{\mathrm{N}^2 - 2\mathrm{N}\sin 3\alpha + 1}$, and $Q = \arctan\left[2\mathrm{N}\cos 3\alpha/(\mathrm{N}^2 - 1)\right] + 3\alpha + 6\beta + \pi/2$. The sum of the squares of the amplitudes of the quantum states $|\psi\rangle$ remains constant when α and β are tuned, with $A_1^2 + A_2^2 = 2\mathrm{N}^2 + 2$.

Experimentally, we first select two-flake (N = 1) stacked GaSe crystal with thickness of $t = l_c/2 = 1.78$ μm. Here, the normalized quantum state $|\psi\rangle$ can be expressed as

$$|\psi\rangle = \cos\left(\frac{\pi/2 - 3\alpha}{2}\right)|RR\rangle_{s,i} + \cos\left(\frac{\pi/2 + 3\alpha}{2}\right)e^{-i(3\alpha+6\beta)}|LL\rangle_{s,i}. \tag{7}$$

The quantum states are reconstructed via tomographic measurements under different α and β values [Fig. 4(b); Supplemental Material [40] Figs. S6 and S7]. At $\beta = 0°$, two amplitudes A_1 and A_2 obtained from the reconstructed density matrices find good agreement with our theoretical model, following a sinusoidal relationship with α [Fig. 4(c)]. At $\alpha = 0°$, the phase Q of the generated quantum states $|\psi\rangle$ varies linearly with β, as expected [Fig. 4(d)]. By jointly tuning α and β, the quantum states can be continuously controlled—from maximally polarization-entangled states to fully separable states with arbitrary phases—while maintaining a constant generation rate. In addition, by increasing flake number N within each section, the photon-pair brightness can be enhanced scaling as $N^2 + 1$. We achieve a coincidence rate of ~1780 Hz in a twin-twisted GaSe crystal with $N = 3$. [Fig. 4(e) and Supplemental Material [40] Fig. S8].

In summary, we have introduced a new design of SPDC sources based on twin-twisted vdW crystal. This design enables a compact entangled photon-pair source with both high brightness and unprecedented quantum state tunability in twin-twisted GaSe crystal (Supplemental Material [40] Tables S1 and S2). The twist-engineered platform is in principle highly compatible for integrating with a microelectromechanical system (MEMS) for *in situ* quantum state tunability [17,47], optical microcavities for enhanced SPDC efficiency [48,49], and photonic circuits for on-chip quantum photonic applications [50,51]. Our study provides a transformative framework for tunable quantum photonics and paves the way toward developing vdW crystals as promising candidates for next-generation compact and integrated quantum light sources.

Acknowledgments—This work was supported by the National Key R&D Program of China (No. 2021YFA1400200, No. 2022YFA1403504, and No. 2024YFA1409600), National Natural Science Foundation of China (No. 52025023, No. 12422406, No. 12374167, No. 12574214, No. 12404355, No. T2325022, and No. U23A2074), the Innovation Program for Quantum Science and Technology (No. 2021ZD0303200 and No. 2021ZD0301500), Guangdong Major Project of Basic and Applied Basic Research (No. 2021B0301030002).

Data availability—The data that support the findings of this article are not publicly available. The data are available from the authors upon reasonable request.

[1] D. C. Burnham and D. L. Weinberg, Observation of simultaneity in parametric production of optical photon pairs, Phys. Rev. Lett. **25**, 84 (1970).

[2] Y. H. Shih and C. O. Alley, New type of Einstein-Podolsky-Rosen-Bohm experiment using pairs of light quanta produced by optical parametric down conversion, Phys. Rev. Lett. **61**, 2921 (1988).

[3] P. G. Kwiat, K. Mattle, H. Weinfurter, A. Zeilinger, A. V. Sergienko, and Y. Shih, New high-intensity source of polarization-entangled photon pairs, Phys. Rev. Lett. **75**, 4337 (1995).

[4] P. G. Kwiat, E. Waks, A. G. White, I. Appelbaum, and P. H. Eberhard, Ultrabright source of polarization-entangled photons, Phys. Rev. A **60**, R773 (1999).

[5] A. Zeilinger, Experiment and the foundations of quantum physics, Rev. Mod. Phys. **71**, S288 (1999).

[6] N. Gisin and R. Thew, Quantum communication, Nat. Photonics **1**, 165 (2007).

[7] V. Scarani, H. Bechmann-Pasquinucci, N. J. Cerf, M. Dusek, N. Lütkenhaus, and M. Peev, The security of practical quantum key distribution, Rev. Mod. Phys. **81**, 1301 (2009).

[8] J. L. O'Brien, A. Furusawa, and J. Vuckovic, Photonic quantum technologies, Nat. Photonics **3**, 687 (2009).

[9] A. Aspuru-Guzik and P. Walther, Photonic quantum simulators, Nat. Phys. **8**, 285 (2012).

[10] H. S. Zhong *et al.*, 12-photon entanglement and scalable scattershot boson sampling with optimal entangled-photon pairs from parametric down-conversion, Phys. Rev. Lett. **121**, 250505 (2018).

[11] L. Li *et al.*, Metalens-array-based high-dimensional and multiphoton quantum source, Science **368**, 1487 (2020).

[12] T. Santiago-Cruz, S. D. Gennaro, O. Mitrofanov, S. Addamane, J. Reno, I. Brener, and M. Chekhova, Resonant metasurfaces for generating complex quantum states, Science **377**, 991 (2022).

[13] V. Sultanov, A. Kavcic, E. Kokkinakis, N. Sebastián, M. V. Chekhova, and M. Humar, Tunable entangled photon-pair generation in a liquid crystal, Nature (London) **631**, 294 (2024).

[14] A. Autere, H. Jussila, Y. Y. Dai, Y. D. Wang, H. Lipsanen, and Z. P. Sun, Nonlinear optics with 2D layered materials, Adv. Mater. **30**, 1705963 (2018).

[15] C. Trovatello *et al.*, Optical parametric amplification by monolayer transition metal dichalcogenides, Nat. Photonics **15**, 6 (2021).

[16] A. R. P. Montblanch, M. Barbone, I. Aharonovich, M. Atatüre, and A. C. Ferrari, Layered materials as a platform for quantum technologies, Nat. Nanotechnol. **18**, 555 (2023).

[17] H. N. Tang, Y. Wang, X. Ni, K. Watanabe, T. Taniguchi, P. Jarillo-Herrero, S. Fan, E. Mazur, A. Yacoby, and Y. Cao, On-chip multi-degree-of-freedom control of two-dimensional materials, Nature (London) **632**, 1038 (2024).

[18] B. Kim, J. C. Jin, Z. Wang, L. He, T. Christensen, E. J. Mele, and B. Zhen, Three-dimensional nonlinear optical materials from twisted two-dimensional van der Waals interfaces, Nat. Photonics **18**, 91 (2024).

[19] M. Zhao, Z. Ye, R. Suzuki, Y. Ye, H. Zhu, J. Xiao, Y. Wang, Y. Iwasa, and X. Zhang, Atomically phase-matched second-harmonic generation in a 2D crystal, Light **5**, e16131 (2016).

[20] J. Shi *et al.*, $3RMoS_2$ with broken inversion symmetry: A promising ultrathin nonlinear optical device, Adv. Mater. **29**, 1701486 (2017).

[21] J. Yu *et al.*, Giant nonlinear optical activity in two-dimensional palladium diselenide, Nat. Commun. **12**, 1083 (2021).

[22] I. Abdelwahab *et al.*, Giant second-harmonic generation in ferroelectric $NbOI_2$, Nat. Photonics **16**, 644 (2022).

[23] X. Y. Xu, C. Trovatello, F. Mooshammer, Y. M. Shao, S. Zhang, K. Y. Yao, D. N. Basov, G. Cerullo, and P. J. Schuck, Towards compact phase-matched and waveguided nonlinear optics in atomically layered emiconductors, Nat. Photonics **16**, 698 (2022).

[24] N. N. Mao *et al.*, Giant nonlinear optical response via coherent stacking of in-plane ferroelectric layers, Adv. Mater. **35**, 2210894 (2023).

[25] J. J. Qi *et al.*, Stacking-controlled growth of rBN crystalline films with high nonlinear optical conversion efficiency up to 1%, Adv. Mater. **36**, 2303122 (2024).

[26] B. Qin *et al.*, Interfacial epitaxy of multilayer rhombohedral transition-metal dichalcogenide single crystals, Science **385**, 99 (2024).

[27] Q. Guo *et al.*, Ultrathin quantum light source with van der Waals $NbOCl_2$ crystal, Nature (London) **613**, 53 (2023).

[28] M. A. Weissflog *et al.*, A tunable transition metal dichalcogenide entangled photon-pair source, Nat. Commun. **15**, 7600 (2024).

[29] J. G. Feng *et al.*, Polarization-entangled photon-pair source with van der Waals 3R-WS_2 crystal, Elight **4**, 16 (2024).

[30] Y. L. Tang *et al.*, Quasi-phase-matching enabled by van der Waals stacking, Nat. Commun. **15**, 9979 (2024).

[31] Q. B. Guo, Y. K. Wu, D. Zhang, Q. H. Zhang, G. C. Guo, A. Alù, X. F. Ren, and C. W. Qiu, Polarization entanglement enabled by orthogonally stacked van der Waals $NbOCl_2$ crystals, Nat. Commun. **15**, 10461 (2024).

[32] L. Kallioniemi, X. Lyu, R. H. He, A. Rasmita, R. H. Duan, Z. Liu, and W. B. Gao, Van der Waals engineering for quantum-entangled photon generation, Nat. Photonics **19**, 142 (2025).

[33] H. D. Liang, T. Gu, Y. C. Lou, C. Y. Yang, C. J. Ma, J. J. Qi, A. A. Bettiol, and X. L. Wang, Tunable polarization entangled photon-pair source in rhombohedral boron nitride, Sci. Adv. **11**, eadt3710 (2025).

[34] X. Lyu, L. Kallioniemi, H. Hong, R. Qu, Y. Zhang, J. Zúñiga-Perez, K. H. Liu, and W. B. Gao, A tunable entangled photon-pair source based on a Van der Waals insulator, Nat. Commun. **16**, 1899 (2025).

[35] C. Trovatello *et al.*, Quasi-phase-matched up- and down-conversion in periodically poled layered semiconductors, Nat. Photonics **19**, 291 (2025).

[36] H. Hong, C. Huang, C. Ma, J. Qi, X. Shi, C. Liu, S. Wu, Z. Sun, E. Wang, and K. Liu, Twist phase matching in two-dimensional materials, Phys. Rev. Lett. **131**, 233801 (2023).

[37] C. L. Tang and H. Rabin, Selection rules for circularly polarized waves in nonlinear optics, Phys. Rev. B **3**, 4025 (1971).

[38] Y. K. Wu, Y. T. Tang, Z. X. Hu, L. T. Feng, G. C. Guo, X. F. Ren, and G. X. Li, Optical spin-orbit interaction in spontaneous parametric downconversion, Optica **10**, 538 (2023).

[39] C. J. Ma *et al.*, Strong chiroptical nonlinearity in coherently stacked boron nitride nanotubes, Nat. Nanotechnol. **19**, 1299 (2024).

[40] See Supplemental Material at http://link.aps.org/supplemental/10.1103/wp59-zvvb for additional experiment and details, which includes Refs. [41–45].

[41] A. N. Vamivakas, Bahaa E. A. Saleh, A. V. Sergienko, and M. C. Teich, Theory of spontaneous parametric down-conversion from photonic crystals, Phys. Rev. A **70**, 043810 (2004).

[42] G. Kulkarni, J. Rioux, B. Braverman, M. V. Chekhova, and R. W. Boyd, Classical model of spontaneous parametric down-conversion, Phys. Rev. Res. **4**, 033098 (2022).

[43] J. Y. Ma, J. H. Zhang, Y. X. Jiang, T. M. Fan, M. Parry, D. N. Neshev, and A. A. Sukhorukov, Polarization engineering of entangled photons from a lithium niobate nonlinear metasurface, Nano Lett. **23**, 8091 (2023).

[44] W. H. Jia, G. Saerens, Ü. L. Talts, H. Weigand, R. J. Chapman, L. Li, R. Grange, and Y. M. Yang, Polarization-entangled Bell state generation from an epsilon-near-zero metasurface, Sci. Adv. **11**, eads3576 (2025).

[45] V. Sultanov, T. Santiago-Cruz, and M. Chekhova, Flat-optics generation of broadband photon pairs with tunable polarization entanglement, Opt. Lett. **47**, 3872 (2022).

[46] Y. B. Ni, H. X. Wu, C. B. Huang, M. S. Mao, Z. Y. Wang, and X. D. Cheng, Growth and quality of gallium selenide (GaSe) crystals, J. Cryst. Growth **381**, 10 (2013).

[47] H. N. Tang *et al.*, An adaptive moiré sensor for spectro-polarimetric hyperimaging, Nat. Photonics **19**, 463 (2025).

[48] F. Yi, M. L. Ren, J. C. Reed, H. Zhu, J. C. Hou, C. H. Naylor, A. T. C. Johnson, R. Agarwal, and E. Cubukcu, Optomechanical enhancement of doubly resonant 2D optical nonlinearity, Nano Lett. **16**, 1631 (2016).

[49] J. X. Zhao *et al.*, Nonlinear polariton parametric emission in an atomically thin semiconductor based microcavity, Nat. Nanotechnol. **17**, 396 (2022).

[50] A. W. Elshaari, W. Pernice, K. Srinivasan, O. Benson, and V. Zwiller, Hybrid integrated quantum photonic circuits, Nat. Photonics **14**, 285 (2020).

[51] Y. C. Wang, K. D. Jöns, and Z. P. Sun, Integrated photon-pair sources with nonlinear optics, Appl. Phys. Rev. **8**, 011314 (2021).